Blocking Phonon Transport by Structural Resonances in Alloy-Based Nanophononic Metamaterials Leads to Ultralow Thermal Conductivity

Shiyun Xiong,[1,2,*] Kimmo Sääskilahti,[3] Yuriy A. Kosevich,[2,4,†] Haoxue Han,[2] Davide Donadio,[5,‡] and Sebastian Volz[2,§]
[1]Max Planck Institute for Polymer Research, Ackermannweg 10, 55218 Mainz, Germany
[2]CNRS, UPR 288 Laboratoire d'Energétique Moléculaire et Macroscopique, Combustion (EM2C), Ecole Centrale Paris, Grande Voie des Vignes, 92295 Châtenay-Malabry, France
[3]Engineered Nanosystems group, School of Science, Aalto University, P.O. Box 12200, 00076 Aalto, Finland
[4]Semenov Institute of Chemical Physics, Russian Academy of Sciences, 119991 Moscow, Russia
[5]Department of Chemistry, University of California Davis, One Shields Avenue, Davis, California 95616, USA
(Received 6 December 2015; published 8 July 2016)

Understanding the design rules to obtain materials that enable a tight control of phonon transport over a broad range of frequencies would aid major developments in thermoelectric energy harvesting, heat management in microelectronics, and information and communication technology. Using atomistic simulations we show that the metamaterials approach relying on localized resonances is very promising to engineer heat transport at the nanoscale. Combining designed resonant structures to alloying can lead to extremely low thermal conductivity in silicon nanowires. The hybridization between resonant phonons and propagating modes greatly reduces the group velocities and the phonon mean free paths in the low frequency acoustic range below 4 THz. Concurrently, alloy scattering hinders the propagation of high frequency thermal phonons. Our calculations establish a rationale between the size, shape, and period of the resonant structures, and the thermal conductivity of the nanowire, and demonstrate that this approach is even effective to block phonon transport in wavelengths much longer than the size and period of the surface resonant structures. A further consequence of using resonant structures is that they are not expected to scatter electrons, which is beneficial for thermoelectric applications.

DOI: 10.1103/PhysRevLett.117.025503

Controlling heat flow using nanophononic materials and devices is growing more and more appealing due to its broad applications in energy conversion and modern computations, including thermoelectrics, thermal cloaks, thermal logic gates, and thermal diodes [1–8]. For thermoelectric applications, one needs materials with a high electronic power factor, as in crystals, but a low thermal conductivity (TC) as in a glass [9]. Designing the TC of a crystalline system to approach or even be lower than the corresponding amorphous limit remains an open challenge both conceptually and technically [10]. The most common route to reduce TC is to exploit phonon scattering at interfaces in nanostructured composites or superlattices [11–14]. In general, only a limited range of phonon frequencies gets scattered efficiently, typically at a relatively high frequency, above 1–2 THz. Nevertheless, low frequency modes also have a significant contribution to the total TC due to their long mean free path (MFP) [15,16]. The best results along this line were obtained using hierarchical structures in heavy element materials, which introduce scatterers from the mesoscale to the atomic scale [17]. In silicon based materials this approach was followed by synthesizing SiGe nanocomposites [18], superlattices [13], and silicon nanomeshes [19,20]. However, in most cases grain boundaries, inclusions, and pores have a negative impact on electronic transport, thus hampering the thermoelectric performance.

As an alternative, the phonon resonant effect in metamaterials [21,22] has been recently proposed for TC design [23–25]. With a careful design of resonant structures, a set of resonant frequencies can be obtained, evidenced by a set of flat bands in the phonon dispersion. Because of the band anticrossing, the resonances interact with the propagating modes and reduce their phonon group velocities. This method allows for manipulating waves with wavelengths much larger than the structural features of the system [26]: low frequency resonances can be easily introduced with small resonant structures.

Branched nanowires (NWs) have been synthesized by the dislocation-driven mechanism [27] and the vapor-liquid-solid process [28–30]. Standing waves (resonances) can be generated inside the branches due to the total reflection of waves at the end of branches. As a result, branched NWs provide an ideal platform for phonon resonance studies and for low TC design. In this work, we report a systematic study on heat transport in Si based resonant structures. Our molecular dynamics simulations show that branched NWs can indeed produce numerous resonances in a broad frequency range. Those resonances interact with phonons in the main NW and reduce their group velocities. The heat flow in the main NW can be manipulated through the design of adequate resonators. We propose a promising methodology to block phonon

 © 2016 American Physical Society

transport at both low and high frequencies: an extremely low TC of 0.9 $W/m \cdot K$ in SiGe alloy crystalline NWs has been achieved with a combination of the phonon resonant and scattering effects.

We first created NWs in the $\langle 100 \rangle$ orientation with a periodic set of branches outside the NWs. The cross section of the main NW is a square with an edge length $L_e = 4.34$ nm. The branches also have a squared cross section with an edge length $L_{bs} = 1.09$ nm and the height of the branches is set to $L_h = 1.63$ nm. To investigate the effect of the number of branches on thermal transport, we designed a set of NWs with branches on one side, two sides, and four sides of the main NW. Sketches of a two-side branched NW are shown in Figs. 1(a) and 1(b). Simulations are carried out with the LAMMPS code [31]. The atomistic 3D models of the NWs and simulation details can be found in Ref. [32].

We calculated the TCs from equilibrium molecular dynamics simulations. The TC of the one-side, two-side, and four-side branched NWs as a function of the period length is depicted in Fig. 1(d). For reference, the TC of the pristine NW computed with the same approach is 19.8 W/mK. This value is comparable to those obtained in former simulations of a square-section Si NW with a similar small diameter [40]. Experimental estimates for so thin NWs are currently not available, and it is worth stressing that our pristine reference model exhibits perfect flat surfaces, which may not be attainable in experiments [41,42] (see the discussions in Ref. [32]). The TC of branched NWs is much smaller than that of the pristine NW, especially at short period lengths. With the increase of the period length, the TC increases gradually for all cases. Besides, the TC is also reduced when more sides of the NW are branched due to the increased hybridization, which further reduces the group velocity as will be discussed later.

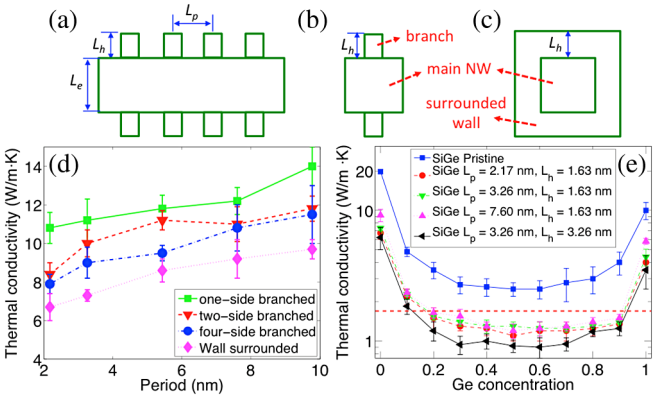

FIG. 1. Side view (a) and cross sections of the two-side branched (b) and square wall surrounded (c) NWs. (d) The TC of branched and wall surrounded NWs varies with the period length. (e) TC as a function of Ge concentration for the pristine and wall surrounded SiGe NWs. The horizontal dashed line presents the calculated TC of an amorphous Si NW of the same size.

Since more branches produce stronger hybridization, we extend the branched structure to square wall surrounded structures [hereafter referred as "surrounded NWs," see Fig. 1(c) and Fig. S1 [32]], to further promote the TC reduction. The thickness of the walls is 1.09 nm while their height is 1.63 nm, i.e., the same dimensions as the studied branches. This structure can be fabricated by the vapor-liquid-solid method with the catalysis diffusion technique [43]. As expected, the TC is further reduced at all periods when compared to all other cases [Fig. 1(d)]. The TC reduction can reach up to 67% at the period of 2.17 nm compared to the one of the pristine NW. The increased anharmonicity at high temperature will reduce the relative TC reduction in resonant NWs. However, due to the strong hindering of low frequency phonons, the relative TC reduction in the surrounded Si NWs with respect to the value of the pristine Si NW can still be 50% at 800 K (Fig. S5 [32]). It is worth noting that the shape of the resonant nanostructures does not affect the TC significantly: the same TC is found in the square and circle wall surrounded Si NWs (Fig. S4 [32]). The TC reduction achieved solely by introducing the resonant structures is comparable to the one achieved in surface engineered NWs [40].

To more deeply understand the origin of the phonon resonant effect, we calculated the phonon dispersion relations and the group velocities v_g of different structures based on harmonic lattice dynamics [44,45]. The comparison of phonon dispersion relations between the pristine structure and the two-side branched structures with $L_p = 2.17$ nm is illustrated in Figs. 2(a)–2(c), where L_h in Fig. 2(c) is twice L_h in Fig. 2(b). With the addition of periodic branches on the main NW surfaces, a series of resonant flat bands crossing the entire Brillouin zone is generated. The resonant modes hybridize with the modes of the main wire due to the band anticrossing effect, which occurs when two modes with the same polarization located on different objects are coupled at the same frequency. Specifically, in our case, if a resonant mode from the pillars has the same polarization as a propagating mode in the main NW, they will hybridize and form two new modes (up and down branches) when their frequencies converge. This mechanism leads to the formation of mini band gaps, the widths of which depend on the coupling or hybridization strength as observed both in theoretical models [46–49], and experimentally [50,51] in acoustic metamaterials.

To provide a picture of how propagating modes hybridize with the resonant modes, we have visualized the modes indicated by the symbols in Fig. 2(b). The hybridization effect between the longitudinal acoustic (LA) mode and the lowest resonance is examined by the eigenvectors. Starting from the mode far away from the resonant frequency (circle), a pure LA mode can be identified from Fig. 2(e): all atoms vibrate along the phonon transport direction z with the same amplitude, following the feature of the LA mode. For the mode on the resonant flat band

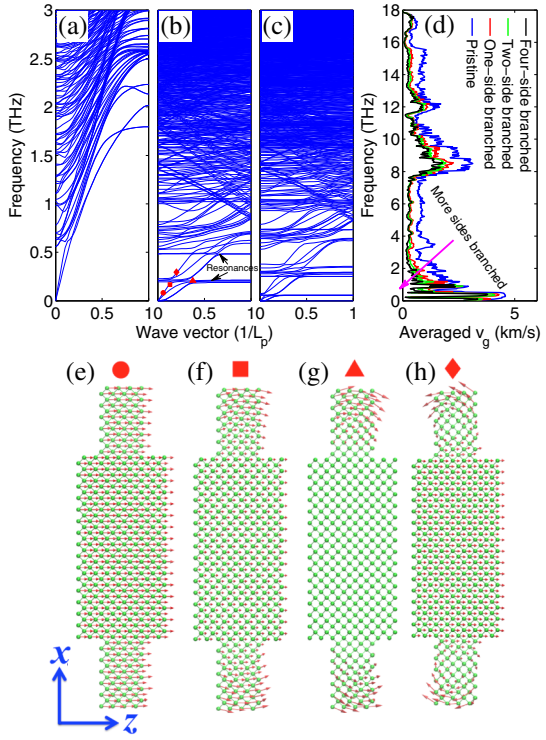

FIG. 2. Phonon dispersion in the frequency range [0, 3] THz for pristine Si NWs (a) and two-side branched Si NWs with $L_h = 1.63$ nm (b) and $L_h = 3.26$ nm (c). Averaged phonon group velocities, where $L_h = 1.63$ nm (d). Visualization of the phonon modes indicated by the circle (e), square (f), triangle (g), and diamond (h) symbols in (b) (drawn with visual molecular dynamics [52]). z is the periodic and the phonon transport direction.

(triangle, a bending mode), it only distributes on the resonant branches; no atoms in the main NW participate in the vibration [Fig. 2(g)]. A hybridized mode resulting from the coupling between the LA mode and the resonant phonon can be identified near to the resonant frequency [square, Fig. 2(f)], where the mismatch in the vibrational amplitudes in the main NW and in the resonator results in a reduced v_g. The effect on the upper side of the resonance is similar to that on the lower side but the atom vibrations in the main NW and on the branches are in opposite phase [Fig. 2(h)]. The enhanced hybridization effect produced by increasing the number of branches is evidenced by the reduced v_g when more surfaces are branched [Fig. 2(d)]. A stronger hybridization enlarges the resonant minigaps as can be seen from the group velocities by polarization in Fig. S3 [32].

The proposed resonant structures offer several advantages in manipulating phonon transport. First, the resonators can produce numerous resonant frequencies in almost the entire frequency range. As a result, the phonon group velocity can be dramatically suppressed at both superwavelength and subwavelength frequencies [Fig. 2(d)]. Second, the resonant frequency can be tuned by altering the branch size and material. The comparison between Figs. 2(b) and 2(c) provides a clear picture of the size effect: when the branch height doubled from 1.63 nm to 3.26 nm, the lowest resonant frequency shifts from 0.2 to 0.06 THz. The increased size of the resonators will also increase the number of resonances. One can therefore adjust the number and the frequency of the resonances by modifying the size of the resonant structures. Consequently, the TC can be easily designed and the heat flow in the main wire can be controlled in a more accurate way. Another important feature of this structure is that the low frequencies can be easily manipulated with small branches, which yields the third advantage of the structure. As discussed above, the lowest resonant frequency can reach down to 0.2 THz with a branch height $L_h = 1.63$ nm and even to 0.06 THz with $L_h = 3.26$ nm. The ability to manipulate such low frequencies with small branches is the key advantage of the resonant mechanism over the scattering mechanism, where the size of scattering sources has to be larger than or comparable to the phonon wavelength. Generally, the phonon scattering mechanism provides an efficient way to block the high frequency phonons while it remains challenging in dealing with phonons with, for example, $f \leq 2$ THz in Si NWs [53] and carbon nanotubes [54]. In contrast with scattering strategies, where the scattering source is located inside the material, the resonant mechanism applies the wave nature of phonons and is produced from a position outside from the main structure. As a result, the resonators are not supposed to scatter electrons. Although there is a substantial modification of the phonon band structure by the resonances, first principles calculations on core-shell NWs [55,56] and elastic theory studies on superlattices [57] have shown that phonon band modifications also have a minor effect on the electrical conductivity.

To achieve the most effective reduction of the TC, one should design a material in which contributions from both the high and low frequency modes are reduced. Since the scattering mechanism is efficient to block high frequency modes and resonances can stop low frequency phonons promisingly, the combination of both effects provides the possibility to block phonons in the full frequency range. Alloying is one of the most efficient ways to scatter high frequency phonons. As a consequence, we have designed a set of surrounded $Si_{1-x}Ge_x$ NWs with Ge concentrations ranging from 0 to 1.

Figure 1(e) reveals the Ge concentration dependent TCs for the pristine and surrounded NWs. The TC of the amorphous Si NW of the same size (1.7 $W/m \cdot K$) calculated at 300 K with the same method is shown as the dashed line for comparison. The TC of pure Si/Ge can be extensively reduced down to 2.5 $W/m \cdot K$ with a Ge concentration in the range of 0.3–0.7. Although extremely low TCs have already been obtained via alloy scattering, those values can still be reduced by a factor of 2 with the introduction of surrounded walls 1.63 nm in height. The

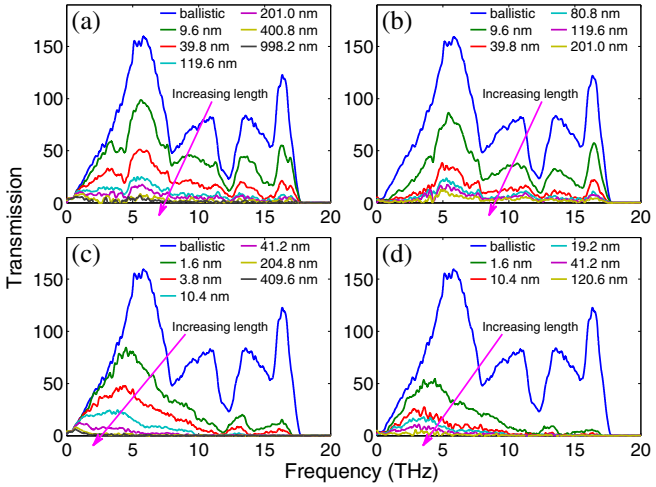

FIG. 3. Length dependent phonon transmission function of (a) pristine Si NWs, (b) surrounded Si NWs, (c) pristine $Si_{0.5}Ge_{0.5}$ NWs, and (d) surrounded $Si_{0.5}Ge_{0.5}$ NWs. The height of the walls is 1.63 nm.

simulated surrounded alloy NWs have TCs below the amorphous Si NW limit except in the case with $x = 0.1$. This indicates that adding resonant structures could be crucial for improving the thermoelectric performance of SiGe alloys. Since the height of the walls can modify the resonant frequency, we also simulated the surrounded SiGe NWs with a doubled wall height. Because of the modification of the low frequency resonances, the TC is further reduced and a value of 0.9 $W/m \cdot K$ is obtained. This extremely low value is about half the corresponding amorphous Si NW TC and 36% of the SiGe alloy NW minimum. In other words, the combination of phonon resonant and scattering mechanisms produces a 22-fold decrease of the pristine Si NW TC.

To quantitatively clarify the respective role of phonon scattering and resonant effects on the TC reduction, we calculated the length dependent phonon transmission functions (Fig. 3) from nonequilibrium molecular dynamics [58,59] (details in Ref. [32]). The ballistic transmission, which is essentially the number of modes in the leads, is shown in all cases to facilitate the comparisons. Because of the anharmonic effect, the transmission of the high frequency phonons in the pristine Si NW decreases when the sample length increases [Fig. 3(a)]. However, ballistic transport can be clearly observed below 1 THz, where the transmission is only slightly decreased even for the NW length of 1 μm. In the surrounded Si NW [Fig. 3(b)], the most noticeable difference with the pristine Si NW case is that the transmissions at frequencies smaller than 4.5 THz are significantly suppressed. This phenomenon demonstrates the importance of the resonant effect at low frequencies, where the number of phonon branches is small but the group velocities are large. Contrary to the features in surrounded Si NWs, the transmission in the $Si_{0.5}Ge_{0.5}$ NW is dramatically reduced at high frequencies

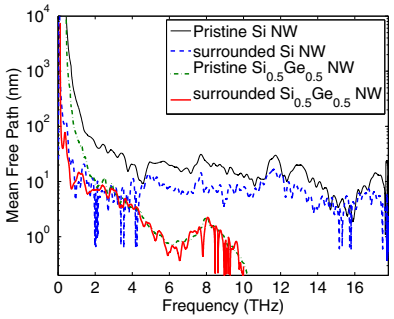

FIG. 4. Frequency resolved mean free paths at 300 K.

even at a very short length [Fig. 3(c)]. However, similar to the pristine Si NW case, ballistic transport is preserved below 1 THz. The strong transmission reductions at low frequencies caused by the resonant effect and at high frequencies due to the scattering effect finally result in reduced transmissions in the whole frequency range in the surrounded $Si_{0.5}Ge_{0.5}$ NWs [Fig. 3(d)]. Note that in the alloyed cases (both pristine and surrounded), the modes at high frequencies (typically above 10 THz) are not propagating modes due to the introduction of heavy Ge atoms. This is evidenced by the extremely low transmission even with a sample length of only 3.8 nm.

From the length dependent transmission functions, we evaluated the frequency resolved phonon MFPs [54,59] using Eq. S4 [32]. As revealed in Fig. 4, the MFP of the pristine Si NW increases rapidly as the frequency shifts below 4 THz. When adding the resonant structure on the surface of the Si NWs, the MFP above 4 THz is reduced roughly by one half. The MFPs of the low frequency phonons are even more reduced by orders of magnitude. Instead, if the scattering sources (Ge atoms) are embedded in the Si NW, the MFP is greatly reduced above 2 THz, while it is not significantly affected below 2 THz. The comparisons among the three samples provide additional evidence that the scattering and resonant mechanisms appear as an ideal combination to design extremely low TCs. This statement is supported by the MFP of surrounded $Si_{0.5}Ge_{0.5}$ NWs, where the MFP in the entire frequency range is reduced by orders of magnitude. The frequency response of the MFPs on resonances and alloys is also revealed by the TC cumulative functions [60] (Fig. S6 [32]).

In conclusion, we have performed molecular dynamics simulations on the TC of Si based resonant NW structures, i.e., branched and wall surrounded NWs. The results reveal that phonon resonance is a powerful TC reduction mechanism. Differing from the commonly adopted scattering method, low frequency phonons can be easily manipulated with small resonators. Both the resonant frequency and strength can be tuned by changing the resonator size, offering the freedom in controlling the heat flow more accurately. The combination of phonon resonant and scattering mechanisms yields a TC of 0.9 $W/m \cdot K$, which

is only 53% of the corresponding Si NW amorphous TC limit and 4.5% of the value of the pristine Si NW. This achievement relies on the hindering of phonon transport in the whole frequency range. The extremely low TC here obtained also supports the potential impact of resonator based structures on thermoelectric conversion.

We thank Samy Merabia for useful discussions. S. X. acknowledges financial funding from the Alexander von Humboldt Foundation. Simulations are performed on the cluster IGLOO of Ecole Centrale Paris and cluster HYDRA from Rechenzentrum Garching of the Max Planck Society (MPG).

*xiongshiyun216@163.com
†yukosevich@gmail.com
‡ddonadio@ucdavis.edu
§sebastian.volz@ecp.fr

[1] M. Maldovan, Sound and heat revolutions in phononics, Nature (London) **503**, 209 (2013).
[2] L. Wang and B. Li, Thermal logic gates: Computation with phonons, Phys. Rev. Lett. **99**, 177208 (2007).
[3] B. Li, L. Wang, and G. Casati, Thermal diode: Rectification of heat flux, Phys. Rev. Lett. **93**, 184301 (2004).
[4] R. Schittny, M. Kadic, S. Guenneau, and M. Wegener, Experiments on transformation thermodynamics: Molding the flow of heat, Phys. Rev. Lett. **110**, 195901 (2013).
[5] N. Li, J. Ren, L. Wang, G. Zhang, P. Hänggi, and B. Li, Colloquium: Phononics: Manipulating heat flow with electronic analogs and beyond, Rev. Mod. Phys. **84**, 1045 (2012).
[6] J. Gomis-Bresco, D. Navarro-Urrios, M. Oudich, S. El-Jallal, A. Griol, D. Puerto, E. Chavez, Y. Pennec, B. Djafari-Rouhani, F. Alzina, A. Martinez, and C. M. S. Torres, A one-dimensional optomechanical crystal with a complete phononic band gap, Nat. Commun. **5**, 5452 (2014).
[7] H. Han, L. G. Potyomina, A. A. Darinskii, S. Volz, and Yu. A. Kosevich, Phonon interference and thermal conductance reduction in atomic-scale metamaterials, Phys. Rev. B **89**, 180301 (2014).
[8] D. G. Cahill, P. V. Braun, G. Chen, D. R. Clarke, S. Fan, K. E. Goodson, P. Keblinski, W. P. King, G. D. Mahan, A. Majumdar, H. J. Maris, S. R. Phillpot, E. Pop, and L. Shi, Nanoscale thermal transport. II. 2003-2012, Appl. Phys. Rev. **1**, 011305 (2014).
[9] G. J. Snyder and E. S. Toberer, Complex thermoelectric materials, Nat. Mater. **7**, 105 (2008).
[10] P. Chen, N. A. Katcho, J. P. Feser, W. Li, M. Glaser, O. G. Schmidt, D. G. Cahill, N. Mingo, and A. Rastelli, Role of surface-segregation-driven intermixing on the thermal transport through planar Si/Ge superlattices, Phys. Rev. Lett. **111**, 115901 (2013).
[11] M. S Dresselhaus, G. Chen, M. Y Tang, R. Yang, H. Lee, D. Wang, Z. Ren, J.-P. Fleurial, and P. Gogna, New directions for low-dimensional thermoelectric materials, Adv. Mater. **19**, 1043 (2007).
[12] B. Poudel, Q. Hao, Y. Ma, Y. Lan, A. Minnich, B. Yu, X. Yan, D. Wang, A. Muto, D. Vashaee, X. Chen, J. Liu, M. S. Dresselhaus, G. Chen, and Z. Ren, High-thermoelectric performance of nanostructured bismuth antimony telluride bulk alloys, Science **320**, 634 (2008).
[13] G. Pernot, M. Stoffel, I. Savic, F. Pezzoli, P. Chen, G. Savelli, A. Jacquot, J. Schumann, U. Denker, I. Mnch, C. Deneke, O. G. Schmidt, J. M. Rampnoux, S. Wang, M. Plissonnier, A. Rastelli, S. Dilhaire, and N. Mingo, Precise control of thermal conductivity at the nanoscale through individual phonon-scattering barriers, Nat. Mater. **9**, 491 (2010).
[14] I. Savic, D. Donadio, F. Gygi, and G. Galli, Dimensionality and heat transport in Si-Ge superlattices, Appl. Phys. Lett. **102**, 073113 (2013).
[15] A. J. Minnich, J. A. Johnson, A. J. Schmidt, K. Esfarjani, M. S. Dresselhaus, K. A. Nelson, and G. Chen, Thermal conductivity spectroscopy technique to measure phonon mean free paths, Phys. Rev. Lett. **107**, 095901 (2011).
[16] K. T. Regner, D. P. Sellan, Z. Su, C. H. Amon, A. J. H. McGaughey, and J. A. Malen, Broadband phonon mean free path contributions to thermal conductivity measured using frequency domain thermoreflectance, Nat. Commun. **4**, 1640 (2013).
[17] K. Biswas, J. He, I. D. Blum, C.-I. Wu, T. P. Hogan, D. N. Seidman, V. P. Dravid, and M. G. Kanatzidis, High-performance bulk thermoelectrics with all-scale hierarchical architectures, Nature (London) **489**, 414 (2012).
[18] G. Joshi, H. Lee, Y. Lan, X. Wang, G. Zhu, D. Wang, R. W Gould, D. C Cuff, M. Y Tang, M. S Dresselhaus, G. Chen, and Z. Ren, Enhanced thermoelectric figure-of-merit in nanostructured p-type silicon germanium bulk alloys, Nano Lett. **8**, 4670 (2008).
[19] J.-K. Yu, S. Mitrovic, D. Tham, J. Varghese, and J. R Heath, Reduction of thermal conductivity in phononic nanomesh structures, Nat. Nanotechnol. **5**, 718 (2010).
[20] J. Tang, H.-T. Wang, D. H. Lee, M. Fardy, Z. Huo, T. P. Russell, and P. Yang, Holey silicon as an efficient thermoelectric material, Nano Lett. **10**, 4279 (2010).
[21] Z. Liu, X. Zhang, Y. Mao, Y. Y Zhu, Z. Yang, C. T Chan, and P. Sheng, Locally resonant sonic materials, Science **289**, 1734 (2000).
[22] Yu. A. Kosevich, Capillary phenomena and macroscopic dynamics of complex two-dimensional defects in crystals, Prog. Surf. Sci. **55**, 1 (1997).
[23] B. L. Davis and M. I. Hussein, Nanophononic metamaterial: Thermal conductivity reduction by local resonance, Phys. Rev. Lett. **112**, 055505 (2014).
[24] H. Honarvar and M. I. Hussein, Spectral energy analysis of locally resonant nanophononic metamaterials by molecular simulations, Phys. Rev. B **93**, 081412 (2016).
[25] Yu. A. Kosevich, Multichannel propagation and scattering of phonons and photons in low-dimensional nanostructures, Phys. Usp. **51**, 848 (2008).
[26] P. Wang, F. Casadei, S. Shan, J. C. Weaver, and K. Bertoldi, Harnessing buckling to design tunable locally resonant acoustic metamaterials, Phys. Rev. Lett. **113**, 014301 (2014).

[27] M. J. Bierman, Y. K. A. Lau, A. V. Kvit, A. L. Schmitt, and S. Jin, Dislocation-driven nanowire growth and eshelby twist, Science **320**, 1060 (2008).
[28] K. A. Dick, K. Deppert, M. W. Larsson, T. Martensson, W. Seifert, L. R. Wallenberg, and L. Samuelson, Synthesis of branched 'nanotrees' by controlled seeding of multiple branching events, Nat. Mater. **3**, 380 (2004).
[29] Y. Jung, D.-K. Ko, and R. Agarwal, Synthesis and structural characterization of single-crystalline branched nanowire heterostructures, Nano Lett. **7**, 264 (2007).
[30] D. Wang, F. Qian, C. Yang, Z. Zhong, and C. M. Lieber, Rational growth of branched and hyperbranched nanowire structures, Nano Lett. **4**, 871 (2004).
[31] S. Plimpton, Fast parallel algorithms for short-range molecular dynamics, J. Comput. Phys. **117**, 1 (1995).
[32] See Supplemental Material at http://link.aps.org/supplemental/10.1103/PhysRevLett.117.025503, which includes Refs. [33–39], for thermal conductivity values, simulation details, and discussions on the shape effect of resonator structures on thermal conductivities, temperature dependent thermal conductivity and thermal conductivity accumulation function with sample length.
[33] F. H. Stillinger and T. A. Weber, Computer simulation of local order in condensed phases of silicon, Phys. Rev. B **31**, 5262 (1985).
[34] K. Ding and H. C. Andersen, Molecular-dynamics simulation of amorphous germanium, Phys. Rev. B **34**, 6987 (1986).
[35] S. Nosé, A molecular dynamics method for simulations in the canonical ensemble, Mol. Phys. **52**, 255 (1984).
[36] W. G. Hoover, Canonical dynamics: Equilibrium phase-space distributions, Phys. Rev. A **31**, 1695 (1985).
[37] R. Kubo, M. Toda, and N. Hashitsume, *Statistical Physics 2* (Springer, Berlin, 1985).
[38] J. Carrete, L. J. Gallego, L. M. Varela, and N. Mingo, Surface roughness and thermal conductivity of semiconductor nanowires: Going below the casimir limit, Phys. Rev. B **84**, 075403 (2011).
[39] D. P. Sellan, E. S. Landry, J. E. Turney, A. J. H. McGaughey, and C. H. Amon, Size effects in molecular dynamics thermal conductivity predictions, Phys. Rev. B **81**, 214305 (2010).
[40] D. Donadio and G. Galli, Atomistic simulations of heat transport in silicon nanowires, Phys. Rev. Lett. **102**, 195901 (2009).
[41] A. I. Hochbaum, R. Chen, R. D. Delgado, W. Liang, E. C. Garnett, M. Najarian, A. Majumdar, and P. Yang, Enhanced thermoelectric performance of rough silicon nanowires, Nature (London) **451**, 163 (2008).
[42] D. Li, Y. Wu, P. Kim, L. Shi, P. Yang, and A. Majumdar, Thermal conductivity of individual silicon nanowires, Appl. Phys. Lett. **83**, 2934 (2003).
[43] J. B. Hannon, S. Kodambaka, F. M. Ross, and R. M. Tromp, The influence of the surface migration of gold on the growth of silicon nanowires, Nature (London) **440**, 69 (2006).
[44] M. Born and K. Huang, *Dynamical Theory of Crystal Lattices* (Clarendon Press, Oxford, 1998).
[45] H. Zhao and J. B. Freund, Lattice-dynamical calculation of phonon scattering at ideal Si-Ge interfaces, J. Appl. Phys. **97**, 024903 (2005).
[46] L. Novotny, Strong coupling, energy splitting, and level crossings: A classical perspective, Am. J. Phys. **78**, 1199 (2010).
[47] Yu. A. Kosevich and E. S. Syrkin, Long wavelength surface oscillations of a crystal with an adsorbed monolayer, Phys. Lett. A **135**, 298 (1989).
[48] A. A. Maznev and V. E. Gusev, Waveguiding by a locally resonant metasurface, Phys. Rev. B **92**, 115422 (2015).
[49] E. A. Garova, A. A. Maradudin, and A. P. Mayer, Interaction of rayleigh waves with randomly distributed oscillators on the surface, Phys. Rev. B **59**, 13291 (1999).
[50] N. Boechler, J. K. Eliason, A. Kumar, A. A. Maznev, K. A. Nelson, and N. Fang, Interaction of a contact resonance of microspheres with surface acoustic waves, Phys. Rev. Lett. **111**, 036103 (2013).
[51] P. J. Beltramo, D. Schneider, G. Fytas, and E. M. Furst, Anisotropic hypersonic phonon propagation in films of aligned ellipsoids, Phys. Rev. Lett. **113**, 205503 (2014).
[52] W. Humphrey, A. Dalke, and K. Schulten, VMD—Visual Molecular Dynamics, J. Mol. Graphics **14**, 33 (1996).
[53] S. Xiong, J. Ma, S. Volz, and T. Dumitrica, Thermally-active screw dislocations in Si nanowires and nanotubes, Small **10**, 1756 (2014).
[54] I. Savić, N. Mingo, and D. A. Stewart, Phonon transport in isotope-disordered carbon and boron-nitride nanotubes: Is localization observable?, Phys. Rev. Lett. **101**, 165502 (2008).
[55] X. Chen, Y. Wang, and Y. Ma, High thermoelectric performance of Ge/Si core-shell nanowires: First-principles prediction, J. Phys. Chem. C **114**, 9096 (2010).
[56] J.-N. Shen, L.-M. Wu, and Y.-F. Zhang, First-principles studies of the TE properties of [110]-Ge/Si core/shell nanowires with different surface structures, J. Mater. Chem. A **2**, 2538 (2014).
[57] S. I. Borisenko, The effect of acoustic phonon confinement on electron scattering in $GaAs/Al_xGa_{1-x}As$ superlattices, Semiconductors **38**, 824 (2004).
[58] K. Sääskilahti, J. Oksanen, J. Tulkki, and S. Volz, Role of anharmonic phonon scattering in the spectrally decomposed thermal conductance at planar interfaces, Phys. Rev. B **90**, 134312 (2014).
[59] K. Sääskilahti, J. Oksanen, S. Volz, and J. Tulkki, Frequency-dependent phonon mean free path in carbon nanotubes from nonequilibrium molecular dynamics, Phys. Rev. B **91**, 115426 (2015).
[60] S. Neogi, J. S. Reparaz, L. F. C. Pereira, B. Graczykowski, M. R. Wagner, M. Sledzinska, A. Shchepetov, M. Prunnila, J. Ahopelto, C. M. Sotomayor-Torres, and D. Donadio, Tuning thermal transport in ultrathin silicon membranes by surface nanoscale engineering, ACS Nano **9**, 3820 (2015).